ELSEVIER International Journal of Mass Spectrometry and Ion Processes 157/158 (1996) 163–174

International Journal of Mass Spectrometry and Ion Processes

Experimental methods to alleviate ion coupling effects in matrix-assisted laser desorption ionization Fourier transform ion cyclotron resonance mass spectrometry

J. Scott Anderson, David A. Laude*

Department of Chemistry and Biochemistry, University of Texas at Austin, Austin TX 78712, USA

Received 26 February 1996; accepted 29 May 1996

Abstract

In Fourier transform ion cyclotron resonance (FT-ICR) mass spectrometry performed at high ion densities, coulombic interactions between ions of similar cyclotron frequencies may lead to coupled cyclotron motions. For ions residing in these modes, a coalescence of closely spaced ion frequencies will result, and the observed spectral line shape of otherwise distinct ion masses has the appearance of a single resonant cyclotron frequency. In this work, we use matrix-assisted laser desorption generated ions to provide examples of ion coupling and its effects on isotopic information. Two separate FT-ICR pulse sequences which alter the applied trap potentials are demonstrated to reverse the effects of ion coupling by reducing the ion density inside the trapped-ion cell. The result is a mass spectrum with a resolved isotopic envelope for previously coupled ion frequencies. Analytical benefits obtained with these pulse sequences when applied to a gramicidin-Dubos sample include a 300% increase in mass resolution and 100% improvement in mass measurement accuracy in the MALDI/FT-ICR spectrum.

Keywords: Ion coupling; FT-ICR; MALDI

1. Introduction

The analytical successes of Fourier transform ion cyclotron resonance (FT-ICR) mass spectrometry are well established. Desirable features such as ultrahigh mass resolution and mass accuracy, and high sensitivity are achieved under optimal experimental conditions. However, unfavorable experimental conditions collectively termed as "space charge" often arise when a large number of ions are retained in the trapped-ion cell as a consequence of inappropriate or uncontrolled ionization or trapping. In these cases, coulombic interactions promote deleterious effects such as line broadening or distortion, and uncalibrated shifts in cyclotron frequency [1–7]. Another possible ramification of large ion populations on the ultimate FT-ICR line shape is the coupling of closely spaced resonant ion frequencies. This phenomenon, referred to in the literature as ion coupling [8], collective oscillation [9], or peak coalescence [10], results from a coulombic attraction between ions of similar cyclotron frequency. Individual ion trajectories which under low ion density conditions are independent, undergo a phase locking or synchronization between constituent ion motions to form a single

* Corresponding author.

PII S0168-1176(96)04405-9

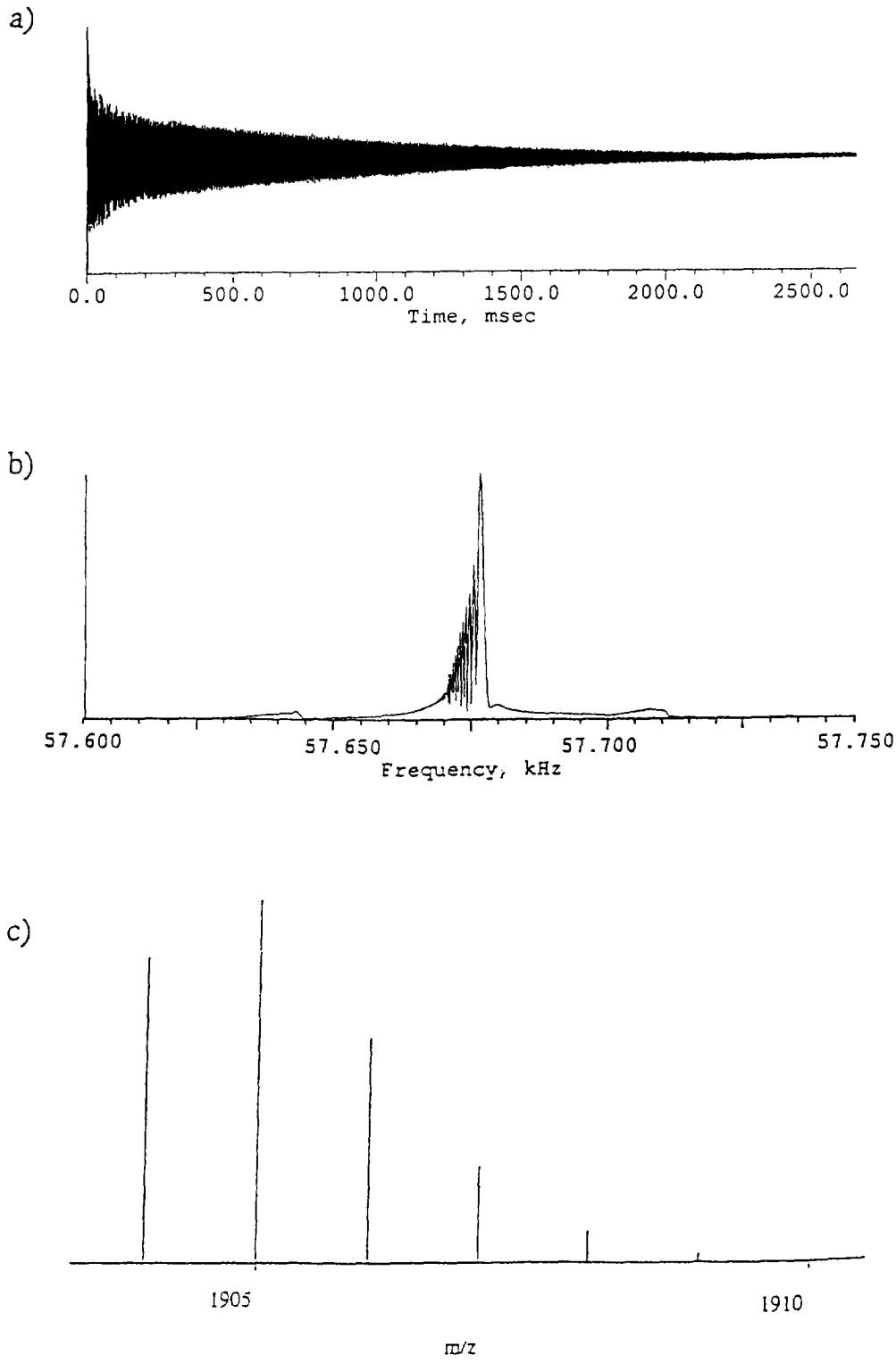
a)
0.0
500.0
1000.0
1500.0
2000.0
2500.0
Time, msec
b)
57.600
57.650
57.700
57.750
Frequency, kHz
c)
1905
1910
m/z

coupled cyclotron motion [11,12]. Under such conditions, the mass spectrum contains a single mass peak for these coupled ion frequencies even though the transient lifetime is sufficient to resolve the individual ions.

Previous experimental studies of ion coupling using FT-ICR have been reported. In one of the first examples, Huang et al. studied low mass ions pairs; N_2 and CO, and naphthalene and its ^{13}C isotope [8]. Using a magnetic field of 0.7 T, these ion pairs have cyclotron frequency differences, $\Delta\omega_c$, of approximately 154 and 650 Hz ($\omega_c/2\pi$) respectively. Employing electron ionization to control the ion population, the authors demonstrate that the degree of coupling is proportional to ion density. In another example, Marshall's group demonstrated ion coupling for small peptides generated by matrix-assisted laser desorption ionization (MALDI) in a 3 T magnetic field [13]. In this case, the cyclotron frequency difference between a partially deuterated leucine enkephalin and its ^{13}C isotope is approximately 1 Hz.

From an analytical standpoint, coupling among ion motions complicates both quantitative and qualitative measures of actual ion abundances and isotopic ratios in certain chemical systems. As described by Mitchell and Smith, the inability to distinguish independent ion clouds results in limited mass resolution, mass accuracy, dynamic range, and incorrect ion abundances [12]. Possible methods to minimize ion coupling and its experimental effects include lowering the ion density inside the trapped-ion cell, increasing the magnetic field (in order to increase the frequency difference between particular ions), or increasing the cyclotron radius to lower the overall space-charge conditions [8,10,13].

In work presented here, we study the coupling of ions in an entire isotopic distribution for a specific MALDI generated protein. The initial motivation for our studies was prompted by the collection of time-domain transients similar to the transient signal in Fig. 1(a). As shown, the transient for the $(M+Na)^+$ isotope packet of the protein gramicidin-D (Dubos) centered around m/z 1905 is observed for a 2.5 s lifetime, which in the absence of inhomogeneous line broadening [14,15] corresponds to a frequency uncertainty of approximately 0.3 Hz. However, the corresponding unapodized frequency spectrum in Fig. 1(b) displays a frequency drift of approximately 10 Hz over the duration of the transient. This frequency drift during data acquisition can be attributed to changing space-charge contributions which are proportional to ion density [4,5]. The ion cloud radial electric field acts to lower the effective magnetic Lorentz force, thereby reducing the unperturbed cyclotron frequency. Computational methods have been devised to correct for this drift in either the frequency [16] or time [17] domain to extract the maximum possible mass resolution.

Of greater concern in the frequency spectrum in Fig. 1(b) is that even with a correction for frequency drift, the isotopic distribution for the protein molecular ion remains unresolved. A comparison with the calculated isotopic distribution in Fig. 1(c) [18] indicates that seven isotopes which should be present are absent in the experimental spectrum. In addition, the coupling phenomenon is exacerbated by the small frequency difference, $\Delta\omega_c \approx (2\pi)30$ Hz, between adjacent gramicidin-D isotopes at a magnetic field strength of 7.2 T.

In this report, we present experimental trapping methods for the MALDI experiment which recover partial isotopic distributions from coupled resonances by alleviating the high ion

Fig. 1. A heterodyne time domain transient for the MALDI generated sodium adduct of gramicidin Dubos protein is shown in (a). The unapodized magnitude-mode Fourier transform of the time domain signal illustrated in (b) displays a shift to lower frequency over the transient lifetime. Coupling among isotope frequencies results in a single frequency peak without the characteristic isotope pattern. A theoretical isotopic distribution for the gramicidin-D adduct is displayed in (c).

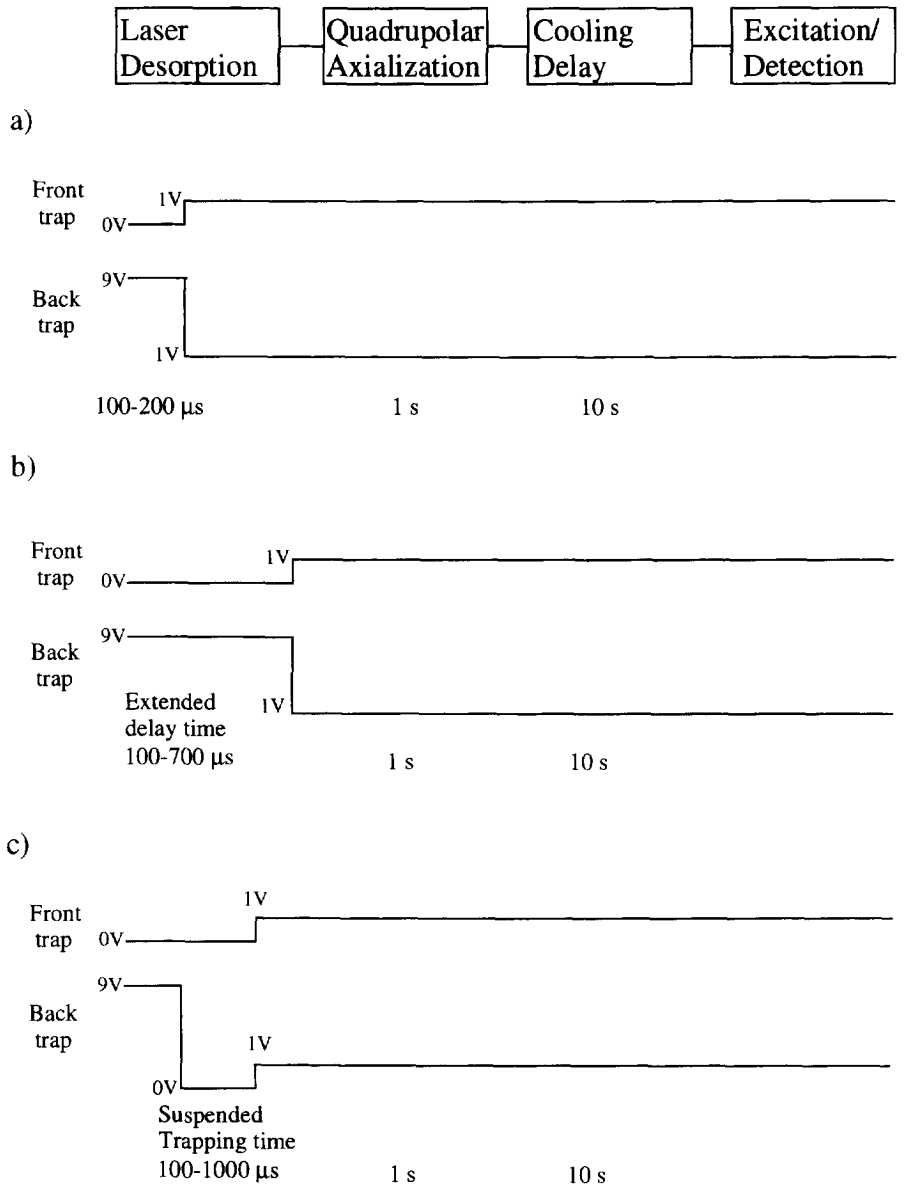

Fig. 2. Pulse sequences used for trapping MALDI ions in the FT-ICR experiment. The general form of gated trapping used to obtain maximum MALDI signal abundance is shown in (a). By increasing the delay time in (b), a smaller portion of the total ion population is retained in the trapped-ion cell. As a result, a much smaller ion population is trapped and coupling is reduced at longer delay times. The sequence in (c) depicts a suspended trapping event used prior to quadrupolar axialization to reduce ion densities. This method also minimizes ion population and eases ion coupling among closely-spaced ion frequencies.

density in the trapped-ion cell. Experimental demonstration of the validity of these procedures is shown for the gramicidin-D molecule.

2. Experimental

The FT-ICR instrumentation employed for all experiments included the following: Finnigan FT/MS version 3.1 Odyssey software and preamplifier (Madison, WI), ENI excitation amplifier (Rochester, NY), and North Hills wideband balun transformer (Syosset, NY). Application of quadrupolar axialization required a switching circuit first used for FT-ICR applications by Schweikhard and Marshall, and employed by many other research groups [19–21]. Individual excitation events were identical in all experiments, and did not include mass-specific quadrupolar axialization [21] or SWIFT isolation [22] for selection or exclusion of certain isotope frequencies.

The superconducting magnet was a 7.2 T vertical bore design constructed by American Magnetics, Inc., (Oak Ridge, TN). This magnet has a limited magnetic homogeneity of 1000 ppm (1 part per thousand) over a 1 cm diameter spherical volume (DSV) at the solenoid center. In an effort to limit the relative magnitude of magnetic inhomogeneity inside the trapped-ion cell, a single-section cylindrical design with diameter 2.79 cm (aspect ratio 1:1) was used for all experiments.

Our MALDI procedure utilized the 337 nm wavelength from a nitrogen laser (Laser Science, Inc., Newton, MA) for ionization. Each laser pulse is focused into a 200 μm fiber optic for direct transmission to the sample surface. Described in detail elsewhere [23,24], this system facilitates laser focusing outside the vacuum chamber and direct placement of the MALDI sample adjacent to the trapped-ion cell.

The matrix/analyte preparation consisted of mixing an abundance of the matrix, 2,5-dihydoxybenzoic acid, with the gramicidin-D protein to achieve an approximate molar concentration ratio of 1500:1. The total amount of protein deposited onto the sample probe tip was in the 1–10 nmol range, with much lower concentrations of analyte residing at the actual desorption sites. Signal generation for this protein was typically consistent for 100 laser pulses per desorption site.

The basic MALDI/FT-ICR experimental pulse sequence consists of a gated trapping scheme in which a potential ramp applied to decelerate ions is followed by establishment of a potential well to trap MALDI generated ions [25]. Gated trapping is required because of the relatively high translational energies (1–10 eV) of desorbed, low mass protein ions [26,27]. Shown in Fig. 2(a), with this method ions enter the trapped-ion cell independent of kinetic energy and experience a large electrostatic potential applied to the rear trap electrode. Under proper deceleration conditions, ion kinetic energies are reduced to near zero kinetic energy. Following deceleration, a static trap potential of 1–2 V is established to trap ions for subsequent quadrupolar axialization, dipolar excitation, and detection.

In an effort to combat ion coupling and the effects illustrated in Fig. 1(b) for the MALDI

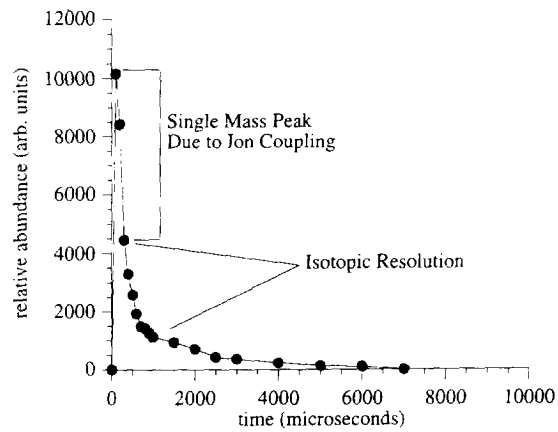

Fig. 3. Measured signal abundance of gramicidin-D is plotted vs. increasing delay times for MALDI gated trapping experiments. Mass spectra which display single line shapes due to ion coupling occur between 100 and 300 μs. At longer delay periods, coupling is reduced and isotopic resolution is achieved.

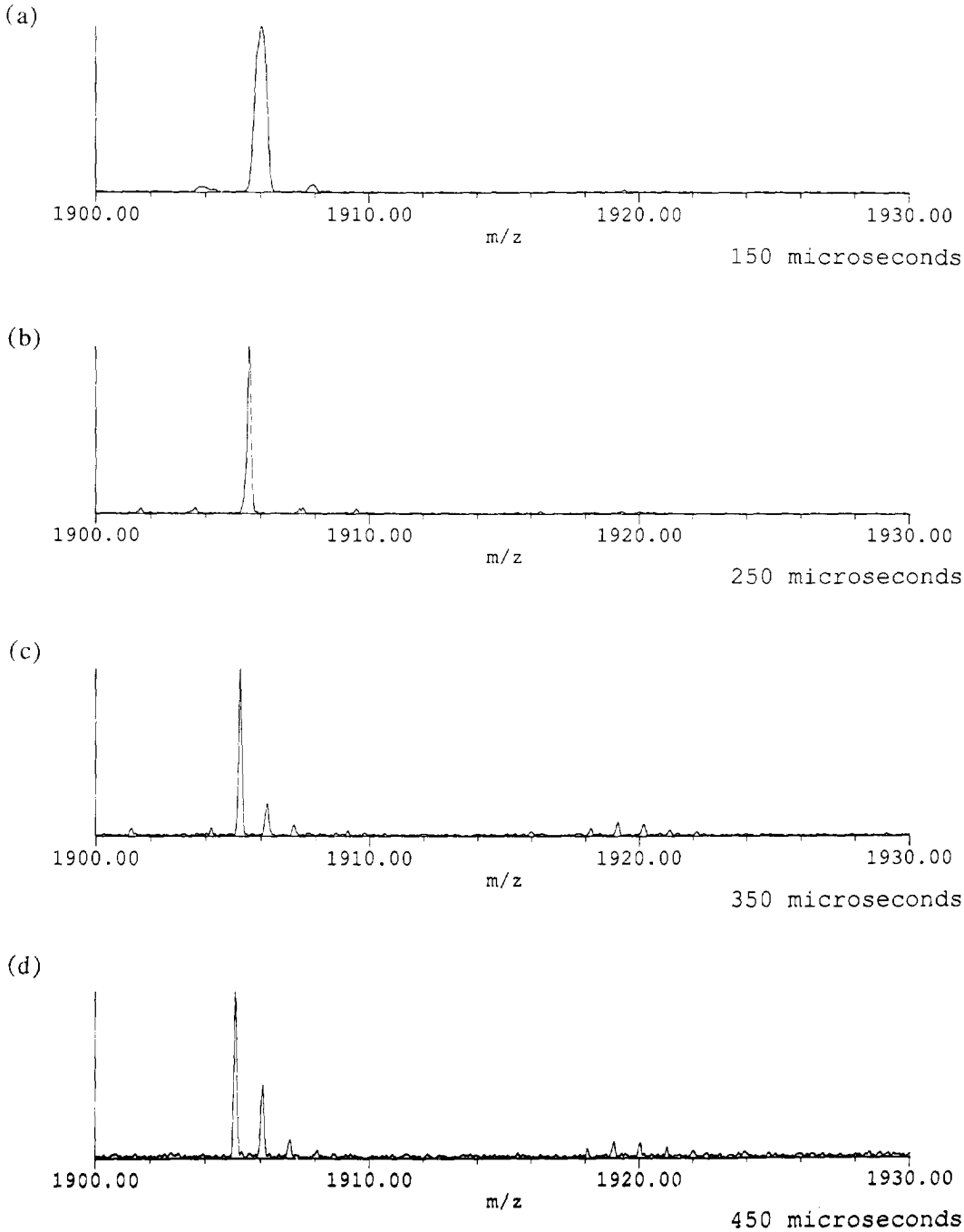

Fig. 4. Mass spectra of the gramicidin-D sodium and potassium adducts at increasing delay times. Quadrupolar axialization, dipolar excitation, and detection conditions (128K data points, 200 kHz bandwidth) are identical for all spectra. Experiments which maximize ion abundance, (a) and (b), yield single mass peaks due to ion coupling. Shown in (c) and (d), uncoupling of isotope frequencies and isotopic resolution becomes feasible at longer delay periods.

experiment, the ion density is reduced by manipulating the applied trap potentials in one of two pulse sequences. In the first method, the delay time for deceleration of MALDI ions is varied. As shown in Fig. 2(b), the deceleration potential is applied for an increasing time so that the fraction of ions that lose sufficient translational kinetic energy to be trapped is reduced. As a result, a much smaller number of ions is retained in the trapped-ion cell prior to detection.

An alternative method employed to reduce ion density is a suspended trapping event [28,29] applied subsequent to deceleration and trapping, but prior to quadrupolar axialization. As illustrated in Fig. 2(c), during the suspended trapping event the trapping electrodes are lowered to ground potential to facilitate axial ejection [30]. Following this event, static trapping voltages of 1–2 V are re-established with a smaller ion population present in the trapped-ion cell.

3. Results and discussion

3.1. Manipulation of ion injection parameters

By employing an increased time delay following laser desorption in the MALDI experiment, a decrease in the ion population and density is obtained. An illustration of this ion loss process is shown in Fig. 3. As the delay time is increased from the microsecond to millisecond timescale, the number of ions trapped decreases as a function of the decreased ion density of the evolving desorption envelope. Fig. 3 indicates that for delay periods between 100 and 300 μs, spectra which exhibit ion coupling are prevalent. The resulting mass spectra using these shorter injection delay conditions is a single line shape representing the coupling of ions in the isotopic packet. However, at longer injection delay periods beyond 300 μs, lower ion densities result and isotopic resolution is achieved.

The mass spectra that generated the abundance profile in Fig. 3, are shown in Fig. 4(a)–(d). The primary ions in these spectra are the $(M+Na)^+$ adduct of *m/z* 1905. As suggested in Fig. 3, coupled ion signals are observed in Fig. 4(a) and (b) when cell ion densities are high. At longer injection delays, the ion cloud density is sufficiently low to yield uncoupled spectra. In Fig. 4(d) at a delay time of 450 μs, uncoupling brings the appearance of four isotope peaks. Further increases in delay time beyond 450 μs reduce signal magnitudes while providing no additional uncoupling or increased resolution of isotopes.

There are several interesting features to note in this series of spectra. First, the possibility that the additional peaks in the mass spectra are sidebands, due either to an electric field modulation between ion clouds or simple experimental artifacts, must be investigated. In Fig. 4(b), the series of adjacent peaks are separated by equally spaced frequencies which are indicative of sidebands rather than genuine ion signals. In contrast to these signals, the peaks in Fig. 4(c) and (d) are likely to correspond to real isotopes because of the unequal frequency difference, $\Delta\omega_c$, between consecutive peaks which represents the sequential addition of the ^{13}C isotope [7]. By plotting the experimental frequency differences from the mass spectra in Fig. 4(b) and (d), sideband and isotope signals can be easily distinguished. This is done in Fig. 5. The data in Fig. 5(a) verify the isofrequency differences between adjacent signals in Fig. 4(b). The 60 Hz spacing found in this case is experimental noise generated by the cryopump. In Fig. 5(b) and (c), the frequency differences, as well as the calculated isomass differences are shown for both gramicidin-D adducts.

The spectra in Fig. 4 improve significantly in analytical performance as ion coupling is reduced. Specifically, spectral resolution and mass measurement accuracy are enhanced. Presented in Fig. 6(a) is a profile of mass resolution taken from the spectra in Fig. 4. The collection of a large ion population at a 150 μs delay time results in a coupled $(M+Na)^+$ adduct peak with mass resolution of approximately 3800. With an

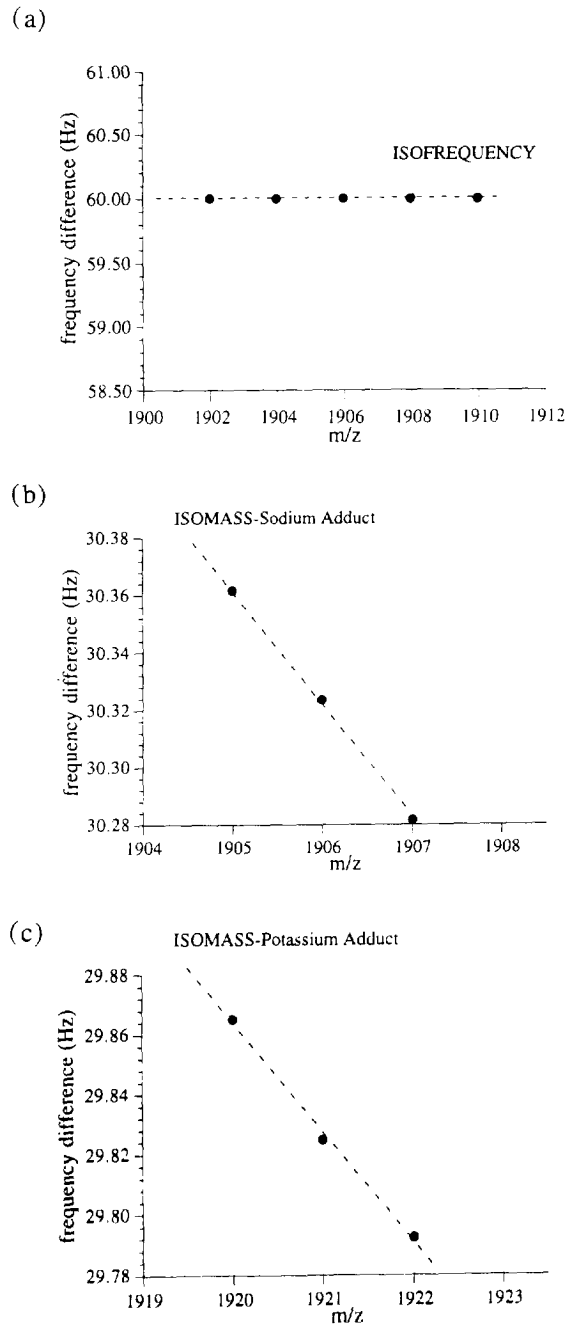

Fig. 5. Frequency differences between adjacent spectral peaks in Figs. 4(b) and 4(d) are plotted vs. increasing ion mass to distinguish sidebands from actual isotope peaks. In (a), the 60 Hz spacing between peaks is an experimental artifact caused by cryopump operation. The slight increases in frequency difference shown in (b) and (c) represent additional ^{13}C isotope masses between real ion signals in the sodium and potassium adducts.

increase in delay time, the spectral quality is improved, isotopic resolution is achieved, and the resolving power increases to a value of 15 000, an improvement of almost 300%.

The data in Fig. 4 also suggest that uncalibrated shifts in cyclotron frequency due to space charge are reduced as ion coupling is eliminated. The coulombic effects in the coupled ion populations evidently contribute significantly to the total radial electric field in the trapped-ion cell [1,4,5]. As previously discussed, the force from this electric field acts to lower the effective magnetic field and consequently the measured

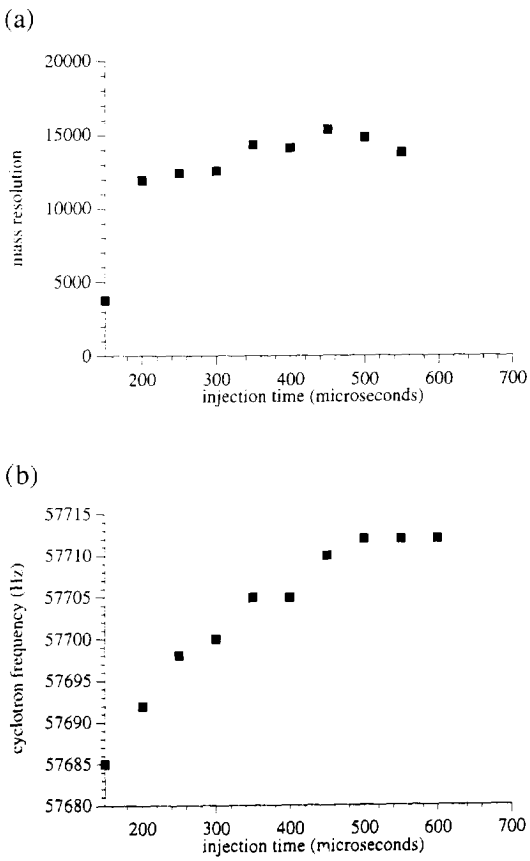

Fig. 6. Using the ^{12}C isotope of the sodium adduct in Figs. 4(a)–(e), the mass resolution (a) and detected cyclotron frequency (b) are plotted with increasing delay times used for the gated trapping event. Mass resolution improves from a value of 3800 to almost 15 000, an increase of almost 300%. The increase in cyclotron frequency signifies an increase in the mass measurement accuracy as the cyclotron frequency shift is reduced. In this case, an improvement from 527 ppm to 22 ppm is observed.

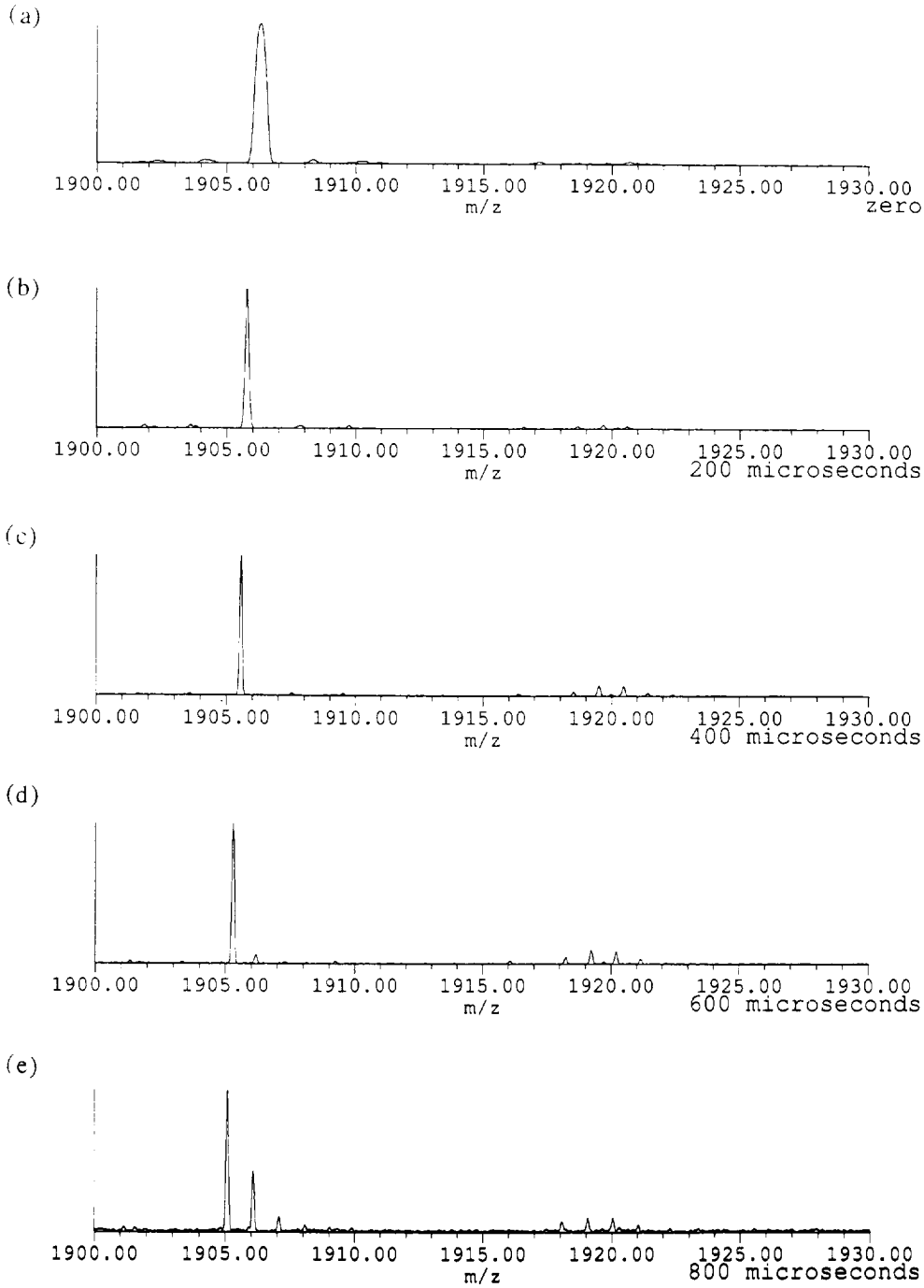

Fig. 7. Using a suspended trapping event prior to quadrupolar axialization, an increase in isotopic resolution and the detected cyclotron frequency for gramicidin-D is observed in the spectra (a)–(d). Similar to the spectra in Fig. 4, identical excitation and detection conditions (128K data points, 200 kHz bandwidth) are employed for all spectra.

cyclotron frequency is shifted to a lower frequency. Illustrated in Fig. 6(b), the increase in cyclotron frequency represents an improvement in mass measurement accuracy corresponding to a shift in frequency from 527 ppm to 22 ppm when compared to an extrapolated single-ion frequency value. In these experiments, the leveling of the cyclotron frequency after a 450 μs delay period suggests that an acceptable ion population is achieved for which coulombic contributions to the radial electric field have minimal affects on the analytical signal.

The sudden appearance of the $(M+K)^+$ isotopic envelope at increased delay times is also of interest. This adduct is completely absent at the large ion densities observed in Fig. 4(a) and (b). There are two possible reasons for the emergence of the $(M+K)^+$ signal. One possible explanation is that a dynamic range limitation exists in the trapped-ion cell for the conditions present in Fig. 4(a) and (b). The large number of $(M+Na)^+$ adduct ions would suppress the smaller signal generated by the $(M+K)^+$ adduct under these circumstances. Another possibility is that although the cyclotron frequency difference between these adducts is rather large, $\Delta\omega_c \approx (2\pi)480$ Hz, coupling between the $(M+Na)^+$ and $(M+K)^+$ adducts has occurred. At lower ion densities, the $(M+Na)^+$ and $(M+K)^+$ ion clouds become uncoupled which results in the emergence of the $(M+K)^+$ isotopic envelope in the mass spectra of Fig. 4(c) and (d). This latter possibility is substantiated by a similar coupling behavior observed for large frequency difference by Huang et al. [8].

3.2. Suspended trapping

In a second approach to uncoupling the isotopic envelope, an initially large ion population is reduced by applying a suspended trapping event prior to quadrupolar axialization. By using the pulse sequence shown in Fig. 2(c), ions which are initially decelerated at the maximum ion abundance possible (100–200 μs delay times), are allowed to expand axially before a static trapping potential is restored. As previously noted, the reduction in ion density should diminish ion coupling and allow isotopic resolution for the gramicidin-D adducts.

The mass spectra in Fig. 7(a)–(d) display a similar trend to the spectra in Fig. 4. Ion coupling is suppressed after a 600 μs suspended trapping time during which a ground potential is applied to the trap electrodes. For these experiments, a maximum number of six isotopes for the $(M+Na)^+$ adduct is observed for the 800 μs suspended trapping event shown in Fig. 7(d).

The improvements in spectral quality using suspended trapping parallel those obtained by varying the delay time during ion injection. By increasing the suspended trapping time in the series of spectra, an obvious improvement in mass resolving power is observed. Using the spectral data from Fig. 7, the plot of mass resolution in Fig. 8(a) illustrates this increase in mass resolution for the ^{13}C isotope of the $(M+Na)^+$ adduct. Beginning at a mass resolution value of 3500 at maximum ion density in Fig. 7(a), mass resolution improves to approximately 16 500 at reduced ion density conditions in Fig. 7(e), an enhancement of approximately 375%.

The increase in the measured cyclotron frequency found in the spectra is plotted in Fig. 8(b). In contrasting the high and low ion density cases, the shift in cyclotron frequency is reduced by 35 Hz. Using the model where radial electric field is due exclusively to the trapping electric field, this reduction yields a shift in mass measurement from 600 ppm to 27 ppm away from the single-ion limit. Here, the mass accuracy improves by almost 100% with the reduction in ion density.

4. Conclusions

We have demonstrated the ability to control the relative number of MALDI generated ions within the trapped-ion cell, and observe the

uncoupling of closely spaced isotope frequencies of gramicidin-D. At the same time, reduced space-charge conditions lead to increased mass resolution and mass measurement accuracy for both the $(M+Na)^+$ and $(M+K)^+$ gramicidin-D adducts. It should be noted that the observed relative abundances of each isotope may not correlate to theoretical abundances because of coupling which may still exist among the closely spaced isotope frequencies. In addition, the observed abundances of the $(M+K)^+$ adduct are diminished because the frequency selected for quadrupolar axialization was optimized for the $(M+Na)^+$ adduct.

The time periods needed for "uncoupled" conditions with both experimental methods vary for each sample and desorption site due to the heterogeneity in the matrix/analyte surface. Uncoupling of the gramicidin adducts at increasing delay or suspended trapping times abruptly occurs once a threshold ion population is achieved in the trapped-ion cell. An important aspect of both ion reduction methods is the similarity in the measured frequency plots. Using an average of three laser shots for each frequency data point in Fig. 6b and Fig. 8b, the leveling in coulomb-induced frequency shift occurs at similar cyclotron frequencies of 57 714 and 57 712 Hz, respectively. More importantly, the onset of ion uncoupling occurs at a common cyclotron frequency, 57 700 ± 3 Hz for the increased delay time method and 57 700 ± 4 Hz in the case of suspended trapping. Quantitative studies to determine the ion population and ion density representative of these ion frequencies would be very useful in predicting the onset of the coupling/decoupling phenomenon. In the case of electron impact ionization, Huang et al. used sample pressure and electron beam cross-section to calculate ion numbers [8]. A complication in the laser desorption experiment is the necessary calibration of the detected image current to calculate a correct ion number in the trapped-ion cell.

Although both trapping methods work well for the gramicidin-D system, there are limitations with the application to higher mass (lower frequency) ions. The ion population of analytes such as bovine insulin b chain (*m/z* 3500 Da) and the intact bovine insulin molecule (*m/z* 5734 Da) can be reduced and the expected increase in cyclotron frequency was observed. However, strong coupling among the isotopes of each molecule still exists, regardless of any experimental manipulation of the trapping potentials. The final experimental result is the single mass peak indicative of strong ion coupling. Corrective measures which may be required to surmount ion coupling for high mass applications include reducing the

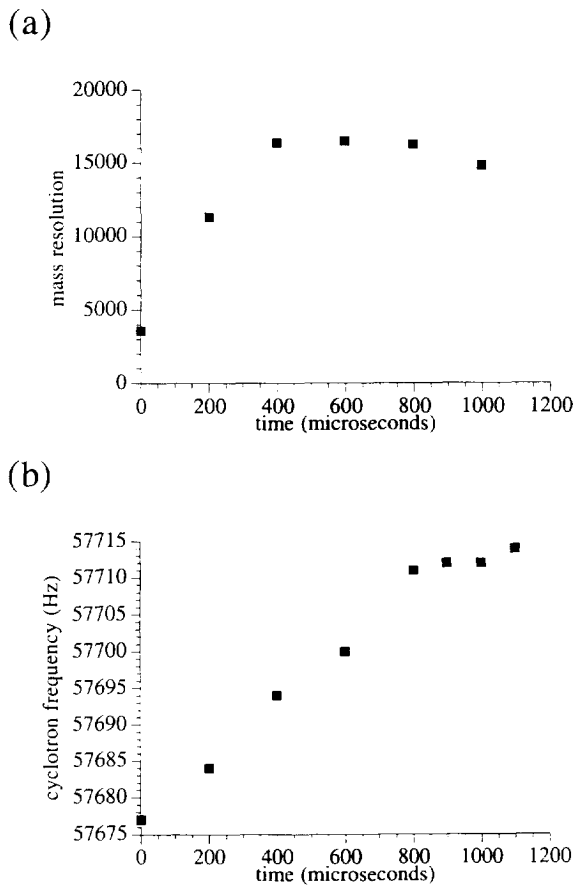

Fig. 8. Using the spectral data from Fig. 7, an increase in mass resolution and measured cyclotron frequency is shown for increasing suspended trapping time. Improvements include an increase in mass resolution from 3500 to 16 500 and mass measurement accuracy from 600 ppm to 27 ppm.

laser desorption energy, using quadrupolar excitation events which are not optimized to generate the greatest detectable signal, enlarging the trapped-ion cell volume to reduce the overall space-charge conditions, exciting ions to larger final cyclotron radius, or increasing the magnetic field strength which in itself minimizes the inclination of larger mass ions to couple simply by shifting the certain mass ion to a larger frequency. A final consideration is the relative importance of field strength versus field quality in any FT-ICR experiment. The opportunity to utilize a larger cell volume in a superconducting magnet of smaller absolute field strength but greater homogeneity may allow greater initial ion densities of gramicidin-D or any closely spaced frequency system to be effectively trapped without the enhanced coupling efficiency.

In choosing a particular method to reduce ion density and acquire improved spectral results, the application of suspended trapping affords the best analytical performance and ease of execution. For examples shown in this work, suspended trapping allows a greater number of isotopes to be detected and a slightly higher mass resolution for the entire isotopic envelope. In addition, employing the variable injection pulse sequence requires knowledge of the desorption profile to properly sample the portion of the desorbed ion packet for which minimal ion coupling occurs. In contrast, the suspended trapping pulse sequence permits a regulation of the ion population to non-coupled conditions regardless of the initial desorption profile.

Acknowledgements

This work was supported by the National Institutes of Health.

References

[1] T.L. Wang and A.G. Marshall, Int. J. Mass Spectrom. Ion Processes, 68 (1986) 287.
[2] S.-P. Chen and M.B. Comisarow, Rapid Commun. Mass Spectrom., 6 (1992) 1.
[3] R.L. Hunter, M.G. Sherman and R.T. McIver, Jr., Int. J. Mass Spectrom. Ion Processes, 50 (1983) 259.
[4] J.B. Jeffries, S.E. Barlow and G.H. Dunn, Int. J. Mass Spectrom. Ion Processes, 54 (1983) 169.
[5] R.C. Dunbar, J.H. Chen and J.D. Hays, Int. J. Mass Spectrom. Ion Processes, 57 (1984) 39.
[6] T.J. Francl, M.G. Sherman, R.L. Hunter, M.J. Locke, W.D. Bowers and R.T. McIver, Jr., Int. J. Mass Spectrom. Ion Processes, 54 (1983) 189.
[7] C.L. Hendrickson, S.C. Beu and D.A. Laude, Jr., J. Am. Soc. Mass Spectrom., 4 (1993) 909.
[8] J. Huang, P.W. Tiedemann, D.P. Land, R.T. McIver and J.C. Hemminger, Int. J. Mass Spectrom. Ion Processes, 134 (1994) 11.
[9] K. Jungmann, J. Hoffnagle, R.G. DeVoe and R.G. Brewer, Phys. Rev., 36 (1987) 3451.
[10] Y. Naito and M. Inoue, J. Mass Spectrom. Soc. Jpn., 42 (1994) 1.
[11] A.J. Peurrung and R.T. Kouzes, Int. J. Mass Spectrom. Ion Processes, 145 (1995) 139.
[12] D.W. Mitchell and R.D. Smith, Phys. Rev. E, 51 (1995) 4366.
[13] L. Pasa-Tolic, S. Guan, G. Jackson, H.S. Kim, Y. Huang and A.G. Marshall, 43rd ASMS Conf. Mass Spectrometry and Allied Topics, Atlanta, GA, 1995, p. 1214.
[14] A.G. Marshall and F.R. Verdun, Fourier Transforms in NMR, Optical, and Mass Spectrometry, Elsevier, Amsterdam, 1990.
[15] M. Comisarow, in H. Hartmann and K.-P. Wanczek (Eds.), Lecture Notes in Chemistry: Ion Cyclotron Resonance Spectrometry II, Springer-Verlag, Berlin, 1982, pp. 484–513.
[16] S. Guan, M.C. Wahl and A.G. Marshall, Anal. Chem., 65 (1993) 3647.
[17] J.E. Bruce, G.A. Anderson, S.A. Hofstadler, B.E. Winger and R.D. Smith, Rapid Commun. Mass Spectrom., 7 (1993) 700.
[18] N. van Eikema Hommes, Mass Cluster version 2.1.
[19] L. Schweikhard, S. Guan and A.G. Marshall, Int. J. Mass Spectrom. Ion Processes 120 (1992) 71.
[20] J.P. Speir, G.S. Gorman, C.C. Pitsenberger, C.A. Turner, P.P. Wang and I.J. Amster, Anal. Chem., 65 (1993) 1746.
[21] C.L. Hendrickson and D.A. Laude, Jr., Anal. Chem., 67 (1995) 1717.
[22] T.-C.L. Wang, T.L. Ricca and A.G. Marshall, Anal. Chem., 58 (1986) 2935.
[23] J.S. Anderson and D.A. Laude, J. Am. Soc. Mass Spectrom., submitted for publication.
[24] J.S. Anderson and D.A. Laude, Proc. 43rd ASMS Conf. Mass Spectrometry and Allied Topics, Atlanta, GA, 1995, p. 793.
[25] J.A. Castoro, C. Koster and C. Wilkins, Rapid Commun. Mass Spectrom., 6 (1992) 239.
[26] R.C. Beavis and B.T. Chait, Chem. Phys. Lett., 181 (1991) 479.
[27] Y. Pan and R.J. Cotter, Org. Mass Spectrom., 27 (1992) 3.
[28] D.A. Laude, Jr., and S.C. Beu, Anal. Chem., 61 (1989) 2422.
[29] J.D. Hogan and D.A. Laude, Jr., Anal. Chem., 62 (1990) 530.
[30] M.L. Gross, S.K. Huang and D.L. Rempel, Int. J. Mass Spectrom. Ion Processes, 70 (1986) 163.